Received 10 June, 2019; | Revised <day> <Month>, <year>; | Accepted <day> <Month>, <year>

DOI: xxx/xxxx

ORIGINAL PAPER

Applying weighted image coaddition to observations of GRB optical afterglows at the D50 telescope in Ondřejov.

Martin Jelínek*[1] | David Alexander Kann[2] | Jan Štrobl[1] | René Hudec[1]

[1] Astronomical Institute of the Academy of Sciences of the Czech Republic, Fričova 298, 251 65 Ondřejov, Czech Republic

[2] Instituto de Astrofísica de Andalucía (CSIC), Glorieta de la Astronomía s/n, 180 08 Granada, Spain

Correspondence
*Corresponding author Email: mates@asu.cas.cz

Present Address
Fričova 298, 251 65 Ondřejov, Czech Republic

Abstract

One of the primary observational objectives of the 0.5m robotic telescope of Ondřejov observatory is the ground-based follow-up of gamma-ray burst triggers. This independent robotic observatory has been in operation since 2008 and has followed up more than a hundred events localized by the *Swift* or *INTEGRAL* satellites.

We describe the use of the weighted coaddition of astronomical images while applying this method to observations of GRB optical afterglows.

We present optical photometric observations of the detected optical afterglows. The collection contains several faint optical afterglows, in some cases a lightcurve is available, in some cases only a single point detection has been achieved. A brief collection of available information is presented for each of the events together with our fitting and analysis.

KEYWORDS:
Gamma-rays: bursts; GRB 080903; GRB 090715B; GRB 120326A; GRB 141225A; GRB 151027B; GRB 160623A; GRB 160625B

1 | INTRODUCTION

Since its first light in 2008, the robotic 0.5 m telescope in Ondřejov has been part of the effort to follow-up gamma-ray burst events. As of now (2019), there have been more than a hundred successful follow-ups of GRB triggers which provided more than a dozen positive detections. We present the method we use to improve the signal-to-noise ratio of our observations, together with a small sample of the weakest optical afterglow detections which have been possible through or have benefitted from this method. This text covers seven optical afterglow detections: GRB 080903, GRB 090715B, GRB 120326A, GRB 141225A, GRB 151027B, GRB 160623A, and GRB 160625B see Fig 1 .

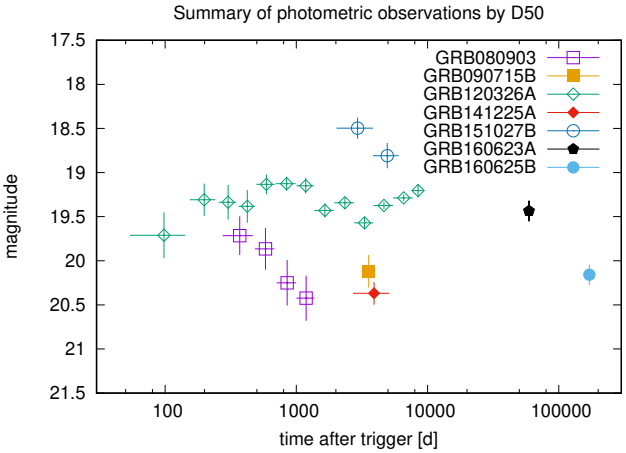

FIGURE 1 All the presented photometric observations.

2 | THE D50 TELESCOPE

D50 is located at the Czech Academy of Science's observatory in Ondřejov, 30 km SW of Prague (at lat: 49°54′ 33.8″N, long: 14°46′52.9″E). The optical path consists of an 0.5 m Newtonian with a parabolic primary mirror of 1975 mm focal length, a 100 mm elliptical secondary and a four-lens TeleVue Paracorr corrector. The telescope was originally equipped with a FLI IMG-1024S CCD camera, which was replaced in 2016 with an Andor iXon Ultra 888 EMCCD (both bursts of 2016 were observed with the Andor); both CCDs have an identical format of 1024×1024 13 μm pixels, which provides a field of view of 20×20 arcmin^2.

The rest of the observatory is historical from the 1960's — the telescope's mount is a refurbished and robotized fork, which originally supported a 63 cm Richter-Slevogt photographic camera and later a coronograph. The wooden sliding roof had also been refurbished and robotized.

The entire observatory is driven by the RTS2 observatory management system Kubánek et al. (2004), the mount was robotized locally with REMOTES (Jakubec et al., 2012) controller and servo motor drives, controlled by RTS2.

2.1 | Archive of observations

D50 archives all its observations in an extensive structured archive, consisting at present of 5 million scientific images. The observed targets are mostly cataclysmic variable stars, but an important portion is occupied by GRB optical follow-ups. The observation programs are known as *Targets*; GRB follow-ups are generated automatically based on information received from the GRB Coordinates Network (GCN) (Barthelmy et al., 1995).

3 | IMAGE PROCESSING

The processing pipeline is available for the image archive to make the data available upon request - a single command would extract images from the archive, search for appropriate calibration frames and apply them, to provide the user with pre-reduced and calibrated images. In case of GRB observations, these images often require further work such as stacking to reveal the optical emission of the event. Note that the GRB observation sequence is universal, without a priori knowledge of the possible object brightness.

3.1 | Weighted coadding

We acknowledge inspiration by Morgan et al. (2008) and in order to achieve optimal coadding of images obtained during observations of optical afterglows we use a weighting scheme. The major difference of the D50 compared to the *Swift* Ultraviolet and Optical Telescope (UVOT) is the presence of the atmosphere together with the related changes of transparency (i.e. local image magnitude zeropoint Z), sky brightness (in terms of image background noise σ) and the presence of variable seeing s. The constant-source optimal coadd would then use

$$w = \frac{10^{Z/2.5}}{\sigma^2 s^2}$$

as weights for the coadd. Similarly to the above mentioned work we then can use the estimated brightness of the object as a supplementary parameter to the weighting, such as

$$w = F_{\mathrm{OT}} \frac{10^{Z/2.5}}{\sigma^2 s^2}.$$

The effective time of the coadded image then must be calculated using these weights as well.

4 | OBSERVATIONS

We used the optimal coadd to improve the signal-to-noise ratio of several detected optical afterglows from the D50 archive. In this section, we present seven of them. The motivation to implement and use the method was mostly because of the variable weather conditions sometimes present during the observations (see Fig. 2). In addition, tracking errors resulting in slightly smeared images can be compensated for by giving worse images less weight. More effects are automatically compensated for: sky brightness, different exposure times, variable seeing and focus.

The calibration of the measurements presented was done against the APASS Catalogue (Henden et al., 2018). The best-fit color transformation of the unfiltered observations is $N_{\mathrm{D50}} \simeq i' + 0.048(r' - i')$, for the R-band observations the best-fit color transformation is $R_{\mathrm{D50}} \simeq r' + 0.013(r' - g')$. The photometry is therefore very close to i' and r', respectively, and has AB zeropoints.

4.1 | GRB 080903

This GRB was detected by *Swift* at 01:12:23 UT, it had a duration of $\mathrm{T}_{90} = 66 \pm 11$ s and the *Swift*/XRT was able to detect its X-ray afterglow for 0.5 days (Evans et al., 2009; Grupe et al., 2008).

The optical afterglow of this GRB was discovered by the 1.5m telescope at Sierra Nevada Observatory (de Ugarte Postigo et al., 2008), and was reported to have been observed by several other groups (Andreev et al., 2008; Guidorzi, Smith, & Gomboc, 2008; Klotz, Boer, Atteia, Grupe, & Schlegel, 2008; Korotkiy, Kryachko, Satovskiy, & Denisenko, 2008; Marshall & Grupe, 2008; Yuan, Rujopakarn, Swan, Smith, &

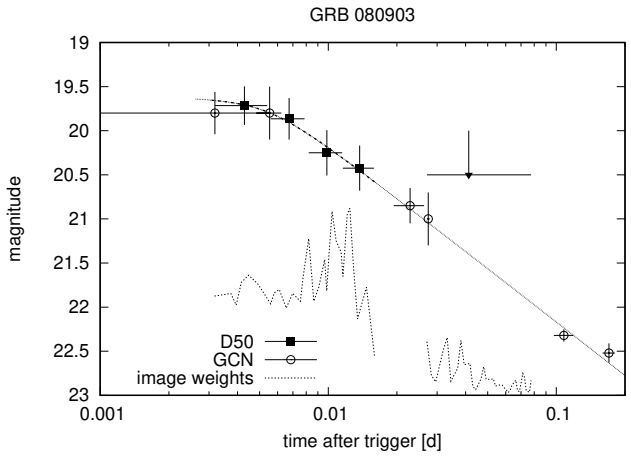

FIGURE 2 Observations of the optical afterglow of GRB 080903, the D50 points are plotted as full symbols, points from the literature as open symbols. The varying conditions during the observations are demonstrated with the value of single image zeropoints.

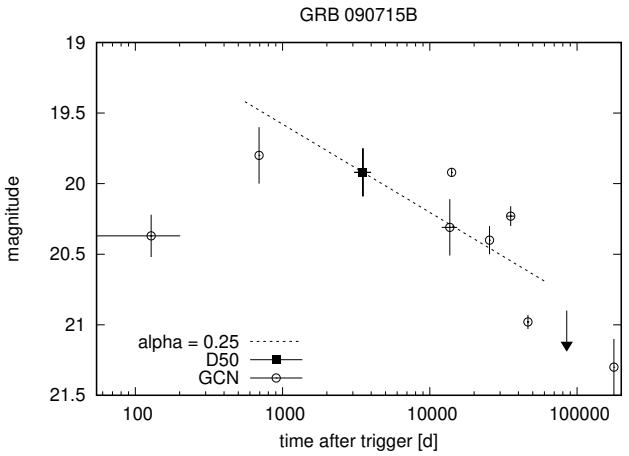

FIGURE 3 Observations of the optical afterglow of GRB 090715B, the D50 points are plotted as full symbols, points from the literature as open symbols.

Guver, 2008). The afterglow is faint, no redshift or host galaxy was reported. There seems to be some discrepancy in the photometry from different groups, e.g., Andreev et al. (2008) seems about a magnitude brighter than our result.

D50 observations started 275 s after the initial trigger and 60 R-band images were obtained with exposure times varying between 10 and 200 s. The conditions during the observations varied with some cirrus passing by. To optimize the image coaddition in order to take into account the varying conditions and exposure times, we used the weighted combination, eventually obtaining 4 photometric points and one limit from the available images, see Table 1 . The lightcurve shows a decay which steepens to a value $\alpha \simeq 0.8$ from a shallower value at the beginning of our observations, similarly to the transition observed in X-rays, only the decay in optical is slower.

4.2 | GRB 090715B

Swift/BAT triggered on this GRB at 21:03:14 UT, the optical afterglow was discovered automatically aboard *Swift* with the UVOT (Vetere et al., 2009). The GRB had two main peaks 10 and 70 s after the trigger followed by continued high energy emission until $\sim$ 300 s after trigger.

Wiersema, Levan, Kamble, Tanvir, & Malesani (2009) with the William Herschel Telescope measured the redshift of $z = 3.00$. In any case, this GRB seems to have been decaying slowly, at first with $\alpha \sim 0.25$, later with $\alpha \sim 0.7$ (Guidorzi et al., 2009). It was also detected in radio by VLA (Chandra & Frail, 2009).

D50 collected two sets of images - the first night it obtained 31 unfiltered images starting 52 min after the trigger. The optical afterglow is easily detected in the coadded image. The second set, from the following night, contains 62 images and the optical afterglow is not detected with a 3-σ limit 21.4.

4.3 | GRB 120326A

GRB 120326A is an unusual burst with a long plateau and a very late rebrightening in both X-ray and optical bands. The gamma-ray duration for this GRB in the 15 – 350keV band is T90 $= 69.5 \pm 8.2s$ Siegel et al. 2013 and the redshift is z = 1.798 (Tello et al., 2012). The burst was followed-up extensively (see the Report by Siegel et al. (2013) for a comprehensive list), and turned out to have a rebrightening peaking at $\sim$30 ks after the trigger.

There is a number of studies for this gamma-ray burst: Urata et al. (2014) deal with high energy emission, Melandri et al. (2014) and Hou et al. (2014) study the optical afterglow behaviour.

D50 started observing 54 s after the GRB and found what seems to be compatible with an onset of the optical afterglow to a peak at $\sim$ 700 s, followed by a decay until $\sim$ 3000 s and again followed by a rise. The complete data spans two hours and comprises 272 unfiltered images. These raw images were combined into 13 coadded frames for photometry. We note that the lightcurve presented by Melandri et al. (2014) shows a different behaviour: the lightcurve decays from the very early times and there is no early rise and peak.

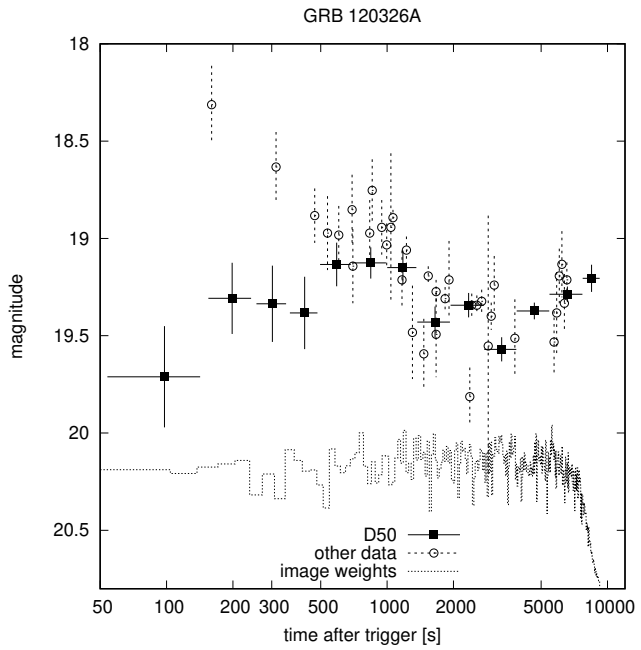

FIGURE 4 Observations of the optical afterglow of GRB 120326A, the D50 points are plotted as full symbols, points from the literature as open symbols.

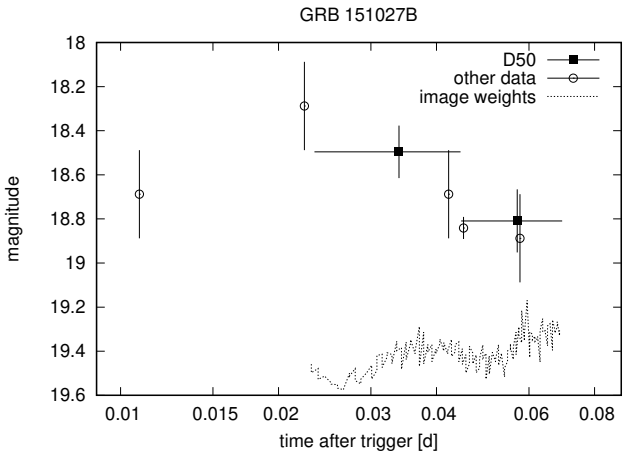

FIGURE 5 Observations of the optical afterglow of GRB 151027B by D50, the photometric points are plotted together with weights of single images used while stacking to illustrate variable conditions.

4.4 | GRB 141225A

This is a GRB discovered by *Swift*/BAT at 23:01:07 UT (D'Avanzo et al., 2014), it was also detected by *Fermi*/GBM (Jenke, 2014). The optical afterglow was discovered by Gorosabel, Hellmich, de Ugarte Postigo, Mottola, & Thoene (2014) with the 1.23 m telescope at Calar Alto, spectroscopic observations with GTC+Osiris revealed a redshift of $z = 0.915$ (Gorosabel, de Ugarte Postigo, et al., 2014).

The optical afterglow was observed by a wide range of instruments including the Liverpool Telescope (Guidorzi, Japelj, & Melandri, 2014), NOT (Malesani, Augusteijn, & Jakobsson, 2014), UVOT (Kuin & D'Avanzo, 2014), the 36 cm telescope at Nanshan (Xu & Gao, 2014), MASTER (Buckley et al., 2014), T60 (Sonbas, Guver, Gogus, Parmaksizoglu, & Dindar, 2014), TAROT (Klotz et al., 2014) and the 2.2 m MPG + GROND (Kann, Schady, & Greiner, 2014).

D50 started observations 45 minutes after the burst trigger and obtained 20 min of images without filter. The combined image yields a positive detection.

4.5 | GRB 151027B

The GRB 151027B was localized by *Swift*/BAT at 22:40:40 UT, the position was promptly improved by the *Swift*/XRT (Ukwatta et al., 2015). The optical afterglow was soon reported by Malesani et al. (2015) and a redshift was determined as $z = 4.063$ with VLT/X-shooter (Xu, Tanvir, Malesani, & Fynbo, 2015).

Greiner et al. (2018) studied this GRB in detail with the 2.2 m MPG telescope + GROND, concluding it is in a good agreement with a relativistic fireball expanding into a constant density interstellar medium.

D50 obtained a series of 133 unfiltered 20 s images starting 33 minutes after the GRB. The faint, slowly decaying afterglow was detected in two coadded images – the first consisted of 61 images, the second of 72 images. During the course of observations, the sky transparency was slowly improving, but the sky brightness was going up. The weighting scheme permitted the use of the all images without losing the signal to noise ratio, see Fig 5 . The two points obtained are compatible with the slow decay shown by Greiner et al. (2018).

4.6 | GRB 160623A

This GRB was discovered by the *Fermi*/GBM instrument and was also detected above 1 GeV with the *Fermi*/LAT (Vianello et al., 2016) as well as Konus-Wind (Frederiks et al., 2016), and was located at Galactic latitude $b = -2.7$. The X-ray afterglow of this burst was found to be surrounded by expanding dust scattering rings with radii between 2 and 9 arcmin, visualizing the Galactic dust for an instant (Pintore et al., 2017).

The optical afterglow of GRB 160623A was observed by the Nordic Optical Telescope (NOT), Very Large Telescope (VLT) with X-shooter, and the Gran Telescopio Canarias (GTC) (Castro-Tirado et al., 2016; Malesani et al., 2016). Hα, S II and N II emission lines were detected at a redshift of $z = 0.367$.

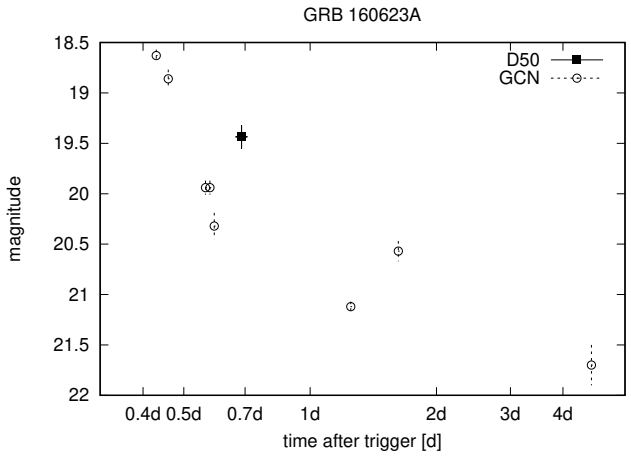

FIGURE 6 The observations of an optical afterglow of GRB 160623A, the D50 point is plotted as a full symbol, points from the literature as open symbols.

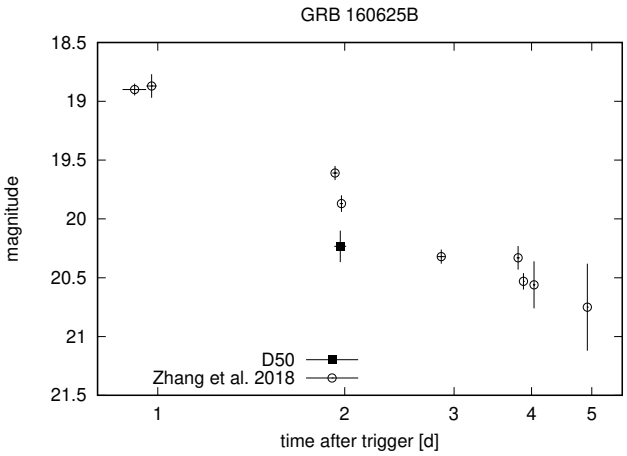

FIGURE 7 GRB 160625A: The observation by D50 in I-band in comparison to the observations in R-band by Zhang et al. (2018).

Observation of the optical afterglow of this GRB poses a particular problem with the presence of a galactic star with $I = 20.6 \pm 0.2$ $\sim 0.7''$ from the GRB location (Malesani et al., 2016). D50 started unfiltered observations 16 h after the GRB trigger and accumulated 1 h of integration time. The telescope, however, does not permit the fine sampling necessary to separate these two objects (they would be separated by $\sim$0.6 pixels). So the value we list in the results is a combined brightness of both objects. In order to reduce the influence of the second nearest star's PSF wings to the photometry of the afterglow, we used an aperture diameter of only 2 pixels, otherwise the photometry could get contamination from this star as well.

Ignoring the difference between Bessel I and SDSS i' bands, assuming the zeropoint difference AB - Vega = 0.45, and subtracting the fluxes, we may obtain a rough estimation of the afterglow value as $i' = 19.7 \pm 0.2$.

4.7 | GRB 160625B

This is a bright and very long gamma-ray burst detected by *Fermi*/GBM, and subsequently observed also by *Fermi*/LAT (Dirirsa & Fermi-LAT Collaboration, 2016), *Swift* performed a tiled search with the XRT and eventually discovered the X-ray afterglow (Melandri et al., 2016).

The optical emission consisted of a bright pulse observed simultaneously with the gamma-ray emission by several ground-based wide-field telescopes (Zhang et al., 2018).

We obtained 350 20 s I-band exposures starting 28 June 2016 at 20:54, i.e. 1.98 days after the GRB trigger. The object is clearly detected in the stacked image. The weighting scheme was used to compensate for the fact that the earliest of the images were obtained with ending twilight and to give less weight to the images which were slightly shifted due to incorrect guiding.

5 | CONCLUSIONS

We demonstrated the use of the weighted coadding of astronomical images and presented seven cases of observations when the optical emission was weak – either because of the delay after the GRB event or because of it was intrinsically dim. All these observations benefitted from the technique, and prove it is useful for further image processing.

REFERENCES

Andreev, M., Sergeev, A., Karpov, N., Khramtsova, M., Petkov, V., & Pozanenko, A. 2008, Jan, *GRB Coordinates Network*, *8175*.

Barthelmy, S. D., Butterworth, P., Cline, T. L., Gehrels, N., Fishman, G. J., Kouveliotou, C., & Meegan, C. A. 1995, Sep, Ap&SS, *231*(1-2), 235-238. doi:

Buckley, D., Potter, S., Kniazev, A. et al. 2014, Jan, *GRB Coordinates Network*, *17245*.

Castro-Tirado, A. J., Valeev, A. F., Jeong, S. et al. 2016, Jan, *GRB Coordinates Network*, *19710*.

Chandra, P., & Frail, D. A. 2009, Jan, *GRB Coordinates Network*, *9695*.

D'Avanzo, P., Beardmore, A. P., Bernardini, M. G. et al. 2014, Jan, *GRB Coordinates Network*, *17229*.

de Ugarte Postigo, A., Castro-Tirado, A. J., Casanova, V., Gorosabel, J., Jelinek, M., & Guerrero, M. 2008, Jan, *GRB Coordinates Network*, *8172*.

Dirirsa, F. F., & Fermi-LAT Collaboration. 2016, Jan, Fermi Observations of the Bright LAT GRB 160625B. Proceedings of the 4th Annual Conference on High Energy Astrophysics in Southern Africa (HEASA 2016). 25-26 August p. 4.

Evans, P. A., Beardmore, A. P., Page, K. L. et al. 2009, Aug, MNRAS, *397*(3), 1177-1201. doi:
Frederiks, D., Golenetskii, S., Aptekar, R. et al. 2016, Jan, *GRB Coordinates Network*, *19554*.
Gorosabel, J., de Ugarte Postigo, A., Thoene, C. C., Tanvir, N., Fynbo, J. P. U., Garcia-Alvarez, D., & Perez-Romero, A. 2014, Jan, *GRB Coordinates Network*, *17234*.
Gorosabel, J., Hellmich, S., de Ugarte Postigo, A., Mottola, S., & Thoene, C. 2014, Jan, *GRB Coordinates Network*, *17230*.
Greiner, J., Bolmer, J., Wieringa, M. et al. 2018, Jun, A&A, *614*, A29. doi:
Grupe, D., Cummings, J. R., Marshall, F. E. et al. 2008, Jan, *GCN Report*, *161*, 1-4.
Guidorzi, C., Cano, Z., Melandri, A. et al. 2009, Jan, *GRB Coordinates Network*, *9677*.
Guidorzi, C., Japelj, J., & Melandri, A. 2014, Jan, *GRB Coordinates Network*, *17231*.
Guidorzi, C., Smith, R. J., & Gomboc, A. 2008, Jan, *GRB Coordinates Network*, *8174*.
Henden, A. A., Levine, S., Terrell, D., Welch, D. L., Munari, U., & Kloppenborg, B. K. 2018, Jun, APASS Data Release 10. American Astronomical Society Meeting Abstracts #232 Vol. 232, p. 223.06.
Hou, S. J., Geng, J. J., Wang, K., Wu, X. F., Huang, Y. F., Dai, Z. G., & Lu, J. F. 2014, Apr, ApJ, *785*(2), 113. doi:
Jakubec, M., Skala, P., Sedlacek, M., Nekola, M., Strobl, J., Blazek, M., & Hudec, R. 2012, Sep, REMOTES: reliable and modular telescope solution for seamless operation and monitoring of various observation facilities. Software and Cyberinfrastructure for Astronomy II Vol. 8451, p. 84511I. doi:
Jenke, P. 2014, Jan, *GRB Coordinates Network*, *17241*.
Kann, D. A., Schady, P., & Greiner, J. 2014, Jan, *GRB Coordinates Network*, *17248*.
Klotz, A., Boer, M., Atteia, J. L., Grupe, D., & Schlegel, D. 2008, Jan, *GRB Coordinates Network*, *8171*.
Klotz, A., Gendre, B., Boer, M., Siellez, K., Dereli, H., Bardho, O., & Atteia, J. L. 2014, Jan, *GRB Coordinates Network*, *17243*.
Korotkiy, S., Kryachko, T., Satovskiy, B., & Denisenko, D. 2008, Jan, *GRB Coordinates Network*, *8173*.
Kubánek, P., Jelínek, M., Nekola, M. et al. 2004, Sep, RTS2 - Remote Telescope System, 2nd Version. E. Fenimore & M. Galassi (Eds.), Gamma-Ray Bursts: 30 Years of Discovery Vol. 727, p. 753-756. doi:
Kuin, N. P. M., & D'Avanzo, P. 2014, Jan, *GRB Coordinates Network*, *17242*.
Malesani, D., Augusteijn, T., & Jakobsson, P. 2014, Jan, *GRB Coordinates Network*, *17232*.
Malesani, D., de Ugarte Postigo, A., de Pasquale, M. et al. 2016, Jan, *GRB Coordinates Network*, *19708*.
Malesani, D., Tanvir, N. R., Xu, D., Harmanen, J., Reynolds, T., & Serrano, P. B. 2015, Jan, *GRB Coordinates Network*, *18501*.
Marshall, F. E., & Grupe, D. 2008, Jan, *GRB Coordinates Network*, *8179*.
Melandri, A., D'Avanzo, P., D'Elia, V. et al. 2016, Jan, *GRB Coordinates Network*, *19585*.
Melandri, A., Virgili, F. J., Guidorzi, C. et al. 2014, Dec, A&A, *572*, A55. doi:
Morgan, A. N., Vanden Berk, D. E., Roming, P. W. A. et al. 2008, Aug, ApJ, *683*(2), 913-923. doi:
Pintore, F., Tiengo, A., Mereghetti, S. et al. 2017, Dec, MNRAS, *472*(2), 1465-1472. doi:
Siegel, M. H., Kuin, N. P. M., Holland, S., Barthelmy, S. D., Burrows, D. N., & Gehrels, N. 2013, Jan, *GCN Report*, *409*.
Sonbas, E., Guver, T., Gogus, E., Parmaksizoglu, M., & Dindar, M. 2014, Jan, *GRB Coordinates Network*, *17240*.
Tello, J. C., Sanchez-Ramirez, R., Gorosabel, J., Castro-Tirado, A. J., Rivero, M. A., Gomez-Velarde, G., & Klotz, A. 2012, Jan, *GRB Coordinates Network*, *13118*.
Ukwatta, T. N., Barthelmy, S. D., Baumgartner, W. H. et al. 2015, Jan, *GRB Coordinates Network*, *18499*.
Urata, Y., Huang, K., Takahashi, S. et al. 2014, Jul, ApJ, *789*(2), 146. doi:
Vetere, L., Cummings, J. R., Breeveld, A., Barthelmy, S. D., Burrows, D. N., Roming, P. W. A., & Gehrels, N. 2009, Jan, *GCN Report*, *236*.
Vianello, G., Dirirsa, F., Omodei, N., Racusin, J. L., Axelsson, M., & Kocevski, D. 2016, Jan, *GRB Coordinates Network*, *19553*.
Wiersema, K., Levan, A., Kamble, A., Tanvir, N., & Malesani, D. 2009, Jul, *GRB Coordinates Network*, *9673*.
Xu, D., & Gao, X. 2014, Jan, *GRB Coordinates Network*, *17236*.
Xu, D., Tanvir, N. R., Malesani, D., & Fynbo, J. 2015, Jan, *GRB Coordinates Network*, *18505*.
Yuan, F., Rujopakarn, W., Swan, H., Smith, D. A., & Guver, T. 2008, Jan, *GRB Coordinates Network*, *8170*.
Zhang, B. B., Zhang, B., Castro-Tirado, A. J. et al. 2018, Nov, *Nature Astronomy*, *2*, 69-75. doi:

How cite this article: Jelínek M., Kann D.A., Jan Štrobl, René Hudec (2019), Seven boring bursts by D50, *Astronomische Nachrichten*, *2019;00:1–6*.

AUTHOR BIOGRAPHY

Martin Jelínek Studied astrophysics in Prague and in Granada. Specializes in robotic telescopes, image processing, high-energy astrophysics, gamma-ray burst follow-up. In the past, he was involved in the robotic system BOOTES in Spain, at present works in Ondřejov with robotic telescopes D50 and BART.

How cite this article: Jelínek M., Kann D.A., Jan Štrobl, René Hudec (2019), Seven boring bursts by D50, *Astronomische Nachrichten*, *2019;00:1–6*.

TABLE 1 Photometric data

start	end	mid [s]	exptime	magnitude
GRB 080903 (*R*-band)				
275	466	370	150 s	19.72 ± 0.22
483	680	582	130 s	19.87 ± 0.24
709	994	852	220 s	20.25 ± 0.26
1002	1370	1186	210 s	20.42 ± 0.26
2340	6693	3566	4000 s	>20.5
GRB 090715B (unfiltered)				
3065	3988	3517	31×20 s	19.92 ± 0.17
84010	85733	85090	62×20 s	> 21.1
GRB 120326A (unfiltered)				
54	142	98	3×20 s	19.71 ± 0.26
155	242	198	3×20 s	19.31 ± 0.18
256	349	302	3×20 s	19.34 ± 0.20
362	483	423	4×20 s	19.38 ± 0.19
497	685	591	6×20 s	19.13 ± 0.11
699	988	843	9×20 s	19.13 ± 0.08
1001	1357	1179	11×20 s	19.15 ± 0.09
1371	1929	1650	17×20 s	19.43 ± 0.08
1942	2748	2345	24×20 s	19.34 ± 0.06
2762	3857	3310	33×20 s	19.57 ± 0.06
3871	5442	4657	47×20 s	19.37 ± 0.04
5456	7694	6575	67×20 s	19.29 ± 0.04
7708	9207	8458	45×20 s	19.21 ± 0.07
GRB 141225A (unfiltered)				
2702	5123	3913	97×20 s	20.37 ± 0.13
GRB 151027B (unfiltered)				
2023	3840	2932	73×20 s	18.50 ± 0.12
3851	5998	4924	86×20 s	18.81 ± 0.14
GRB 160623A (unfiltered)				
57393	61281	59337	25×10 s 119×20 s	19.44 ± 0.12
GRB 160625B (*I*-band)				
170313	166283	173757	347×20 s	19.68 ± 0.13

Start, end and mid times given are relatively to the respective GRB trigger time.